The Dynamic Range of Acidity: Tracking Rules for the Unidirectional Penetration of Cellular Compartments

Lea Assies,[a] Vincent Mercier,[a] Javier López-Andarias,[a] Aurelien Roux,[a] Naomi Sakai,[a] and Stefan Matile*[a]

Labeled ammonium cations with pK_a ~ 7.4 accumulate in acidic organelles because they can be neutralized transiently to cross the membrane at cytosolic pH 7.2 but not at their internal pH < 5.5. Retention in early endosomes with less acidic internal pH was achieved recently using weaker acids of up to pK_a 9.8. We report here that primary ammonium cations with higher pK_a 10.6, label early endosomes more efficiently. This maximized early endosome tracking coincides with increasing labeling of Golgi networks with similarly weak internal acidity. Guanidinium cations with pK_a 13.5 cannot cross the plasma membrane in monomeric form and label the plasma membrane with selectivity for vesicles embarking into endocytosis. Self-assembled into micelles, guanidinium cations enter cells like arginine-rich cell-penetrating peptides and, driven by their membrane potential, penetrate mitochondria unidirectionally despite their high inner pH. The resulting tracking rules with an approximated dynamic range of pK_a change ~ 3.5 are expected to be generally valid, thus enabling the design of chemistry tools for biology research in the broadest sense. From a practical point of view, most relevant are two complementary fluorescent flipper probes that can be used to image the mechanics at the very beginning of endocytosis.

Introduction

In biology, the pK_a of functional groups can change strongly to enable function because the alternative change in pH is usually not possible.[1–7] In enzymatic catalysis, for example, neutral amines are essential to access enamine and iminium chemistry.[8–11] However, alkyl ammonium cations, present in the side chain of lysines (Lys) in proteins, are only weak acids with pK_a ~ 10.5 and remain thus protonated in neutral water (Figure 1A). To produce a neutral amine in neutral water, a second ammonium cation is thus placed nearby, and charge repulsion between the two ammonium cations triggers the release of a proton.[1–4,12–18] This corresponds to an increase of the acidity of one of the two ammonium cations from pK_a ~ 10.5 to pK_a < 8.[8–12] The reverse proximity effect allows to protonate carboxylates in neutral water and provides access to acid catalysis in biology, including glycosidases, proteases and steroid cyclization, folding, assembly, transport, and so on.[19–23]

The dynamic range of acidity describes the difference between the intrinsic pK_a of a given acid and the most extreme pK_a this acid can assume temporarily or permanently in response to demands from the local environment. Naturally, this dynamic range is not infinite and depends on the context. In neutral water, the guanidinium cation in the side chain of arginine is commonly considered beyond the dynamic range of this acid (Figure 1B).

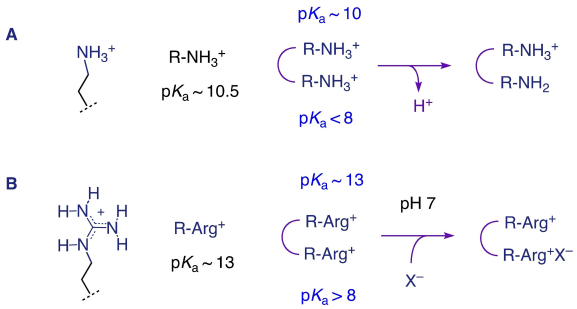

Figure 1. Acidity changes by proximity effects. (A) The acidity of ammonium cations, as in lysine, is sufficient to respond to charge repulsion by deprotonation, producing neutral amines in neutral water. (B) The acidity of guanidinium cations as in arginine (Arg^+) is insufficient for deprotonation in neutral water, which provides access to repulsion-driven ion pairing with anions X^- as a response to charge repulsion.

Examples of deprotonated arginines in protein chemistry are extremely rare. For instance, a pK_a = 8.0 has been reported for pH-sensitive TALK ion channels with a single arginine in a hydrophobic environment.[24] Their intrinsic pK_a is usually given as 12.5, although it has been argued that this is an underestimate, caused by coinciding deprotonation of water, and that pK_a ~ 13.5 could be more reasonable.[25] This pK_a is too high to allow deprotonation in neutral water to reduce charge repulsion between guanidinium cations. The only alternative to minimize charge repulsion within oligoarginines is the tight binding of counterions (Figure 1B).[26] Repulsion-driven ion pairing is very strong, but counterion exchange is facile. This

[a] L. Assies, Dr. V. Mercier, Dr. J. López-Andarias, Prof. A. Roux, Dr. N. Sakai, Prof. S. Matile
School of Chemistry and Biochemistry
NCCR Chemical Biology, University of Geneva
1211 Geneva (Switzerland)
E-mail: stefan.matile@unige.ch

Supporting information for this article is available on the WWW under https://doi.org/10.1002/cbic.202200192

means that counterions will always be bound to oligoarginines in solution, but their nature can easily change. Such repulsion-driven counterion exchange cascades to and from anionic lipids account for the cell-penetrating nature of oligoarginines, which is the most prominent class of cell-penetrating peptides (CPPs, Figure 2A).[26–36] Among charge inverted systems, oligonucleotides stand out. For instance, repulsion-driven ion pairing with cationic amphiphiles produces oligonucleotides that penetrate membranes[37,38] and is used for their delivery into cells (Figure 2B).[36,39–45]

Membrane penetration operating within the dynamic range of acidity is also relevant in chemical biology (Figure 3). In general, permanent monomeric hydrophilic ions fail to cross bilayer membranes because they are insoluble in the apolar core of membranes (Figure 2). However, ammonium cations with low enough pK_a can release their proton on one side of the membrane and pick up a new proton on the other side (Figure 3A).[5–7,46] The reverse is also true for sufficiently basic anions such as carboxylates or fluorides.[47–49]

In the presence of an inside acidic pH gradient from pH 7 to pH 5, ammonium cations can still cross the membrane toward the acidic side by transient deprotonation.[5–7,46,50] However, they cannot return because deprotonation of an ammonium cation of pK_a ~ 10 at pH ~ 5 is beyond the dynamic range of acidity (Figure 3B).[51–58] Thus, the passage of ammonium cation across the membrane with an inside acidic pH gradient is irreversible.

Basic anions such as carboxylates also cross membranes along inside acidic pH gradients. However, they do not accumulate on the acidic side because protonation at low pH is favored (Figure 3B). Although irrelevant in a biological context, unidirectional translocation of carboxylates should occur along inside basic pH gradients because their protonation at pH ~ 9 is beyond the dynamic range of acidity, while ammonium cations

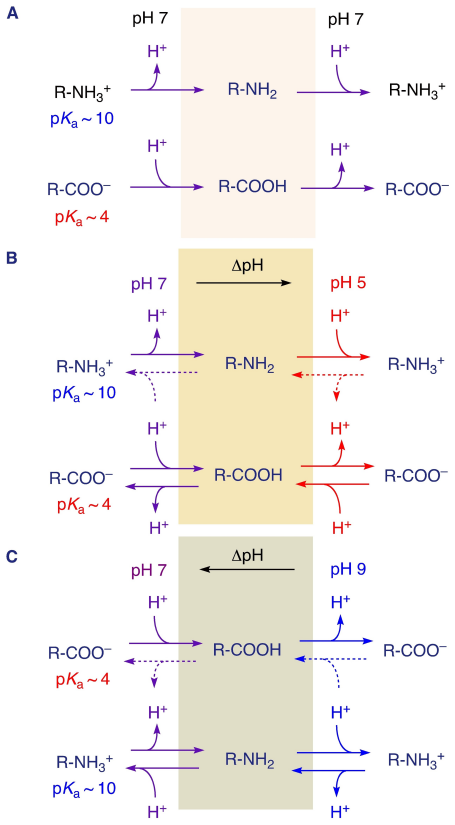

Figure 3. Membrane penetration within the dynamic range of acidity. (A) The acidity of ammonium cations and the basicity of the carboxylate are sufficient to temporarily release and accept a proton and cross membranes as neutral monomers, thereby producing pH gradients in the opposite direction. (B) Unidirectional penetration of membranes with inside acidic pH gradient by transient deprotonation of ammonium cations but not protonation of carboxylates, because the former resist deprotonation at low pH and are retained, while the latter get protonated at low pH and are not retained. (C) The complementary unidirectional penetration with inside basic pH gradient by transient protonation of carboxylate anions but not by deprotonation of amines.

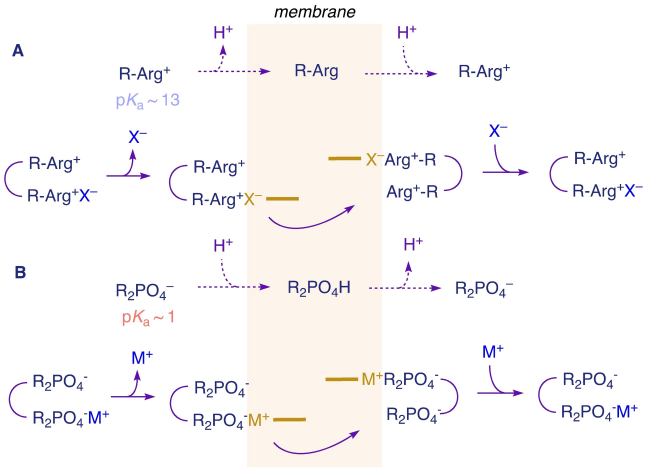

Figure 2. Membrane penetration beyond the dynamic range of acidity. (A) While the acidity of monomeric guanidinium cations is insufficient to temporarily release a proton, oligomeric guanidinium cations (e.g., CPPs) can cross membranes due to repulsion-driven ion pairing and counterion exchange. (B) Same for weakly basic anions: monomers do not, while counterion-activated oligomers do penetrate membranes (e.g., DNA lipoplexes).

should not accumulate on the basic side of the membrane (Figure 3C).

Within cells, lysosomes excel with the steepest inside acidic pH gradient.[51–71] Unidirectional penetration along this strong pH gradient makes fluorescently labeled ammonium cations accumulate in the acidic interior of lysosomes (pH ~ 4.7). This is the molecular basis of most LysoTrackers.[51–58] Morpholinium cations as in **1** with pK_a = 7.4 are most commonly used in LysoTrackers (Figure 4).

During endocytosis, the internal pH gradually decreases from early endosomes to late endosomes (LE) and lysosomes (LY, Figure 5a). While morpholino trackers like **1** still label late endosomes with pH ~ 5.5, they miss early endosomes (EE) with pH ranging from 6.0 to 6.5 (Figure 5C–E). We reasoned that morpholinos **1** with pK_a = 7.4 can enter early endosomes as well as late endosomes, but also exit by transient deprotonation at pH > 6.0 (Figure 5C, D). The labeling of early endosomes thus called for less acidic trackers with pK_a > 7.4. Systematic variation of the pK_a of benzylammonium cations revealed that early

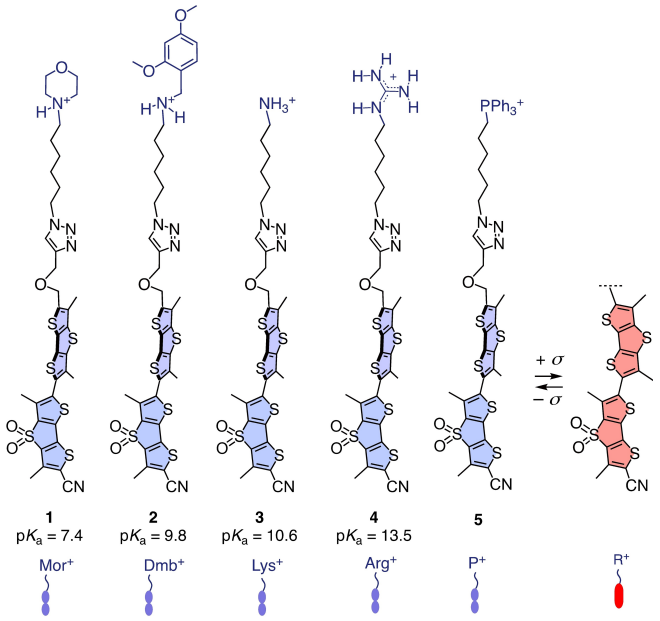

Figure 4. Cationic flipper probes to elucidate tracking rules in cells, with pK_a and symbols used, counterions not indicated; planarization of the twisted probes by mechanical forces σ shifts absorption maxima to the red and increases fluorescence lifetime.

endosome labeling increases with decreasing acidity until the Dmb probe **2** with pK_a = 9.8 (Figures 4, 5D).[51] This result supported that unidirectional penetration along minimalist pH gradients is possible.

Partial tracking of early endosomes with Dmb-Flipper **2** defined the dynamic range of acidity for unidirectional penetration to be larger than pK_a (**2**) – pH (cytosol) and around pK_a (**2**) – pH (EE). Namely, the dynamic range has to be larger than $\Delta pK_a = 2.6$, that is pK_a = 9.8 of the probe **2** minus pH = 7.2 of the cytosol, otherwise the probe could not penetrate acidic organelles from the cytosol by transient deprotonation. However, the dynamic range has to be around $\Delta pK_a = 3.5$, that is pK_a = 9.8 of the probe minus the average pH = 6.3 of early endosomes, otherwise the retention of probe **2** would not be only partial in early endosomes (Figure 5C, D). This $\Delta pK_a = 3.5$ for the dynamic range of acidity to penetrate membranes by transient deprotonation should be quite accurate. With the pH of early endosomes ranging from 6.0 to 6.5, $\Delta pK_a = 3.8$ for probe **2** with pK_a = 9.8 should result in labeling of all and $\Delta pK_a = 3.3$ should give none, while partial labeling is observed. These hypotheses suggested that probes with pK_a = 10.1 could already be sufficient to track all early endosomes. However, going to the limit of $\Delta pK_a = 3.5$ for inward penetration from the cytosol with pH ~7.2, the ideal early endosome tracker would have a pK_a at 7.2 + 3.5 ~ 10.7. In the following, we introduce the collection of probes **1**–**5** to provide experimental support for this conclusion.

MitoTrackers operate with permanent hydrophobic cations.[51,56–58,72–75] Most common are triphenylphosphonium cations as in probe **5**.[58] The outer membrane of mitochondria (MC) is generally permeable for small molecules due to the presence of large pores with little selectivity. The inner mitochondrial membrane is characterized by a strong, inside negative potential.[76] This potential drives fluorophores with permanent positive charge across the membrane, while the release is hindered by the same potential (Figure 5B). This potential-mediated directional penetration suggests that weak cationic acids beyond the dynamic range of acidity around pK_a ~ 10.7 should track mitochondria instead of endolysosomes. In support of this hypothesis, after crossing the plasma membrane (Figure 2A), short CPPs accumulate in mitochondria while longer ones end up in the nucleoli due to cumulative repulsion-driven ion pairing with DNA.[72] In the following, also this hypothesis is validated experimentally.

Trackers **1**, **2** and **5** have been prepared to label intracellular membranes of interest with fluorescent flippers (Figure 4).[58] These bioinspired[77,78] mechanosensitive probes have been introduced to image membrane order as well as changes in membrane tension.[79–81] They are built around two DTT fluorophores that are twisted out of co-planarity by repulsion between sulfurs and methyls around the twistable bond. Physical compression by the surrounding membrane forces the two DTTs into co-planarity. This turns on a push-pull system produced by endo- and exocyclic donors and acceptors, which causes a red shift of the excitation maximum and an increase in fluorescence intensity and lifetime (Figure 5F). Because it is concentration-independent, the response in lifetime to physical compression is most reliable to visualize membrane tension in live cells by fluorescence lifetime imaging microscopy (FLIM). Unlike most alternative membrane probes operating off-equilibrium in the excited state, flippers report physical compression in equilibrium in the ground state.[81] In uniform model membranes, increasing tension is reported as a decrease in lifetime, consistent with lipid decompression. In mixed model membranes and biomembranes, increasing tension is reported as an increase in lifetime, suggesting that the response is dominated by tension-induced membrane reorganization, particularly domain dis/assembly.

In this report, mechanophoric flipper probes **3** and **4** with lower acidity of pK_a = 10.6 and pK_a ~ 13.5 are introduced to develop universal tracking rules for probes that operate by unidirectional penetration and determine the dynamic range of acidity in this context. Being less acidic than **1** and **2**, flippers **3** and **4**, if within the dynamic range of acidity, should accumulate within organelles with less acidic interior, label the inner leaflet of the membrane of these organelles, and image membrane order and tension in this inner leaflet. The envisioned tracking rules should be general and work also for simpler fluorophores as long as they are sufficiently hydrophobic to diffuse across membranes in neutral form.[6] Fluorescent flippers[81] were selected to develop the concept because the resulting membrane tension probes, if operational along the envisioned rules, should provide the chemistry tools to elucidate the mechanics of early stages on endocytosis.

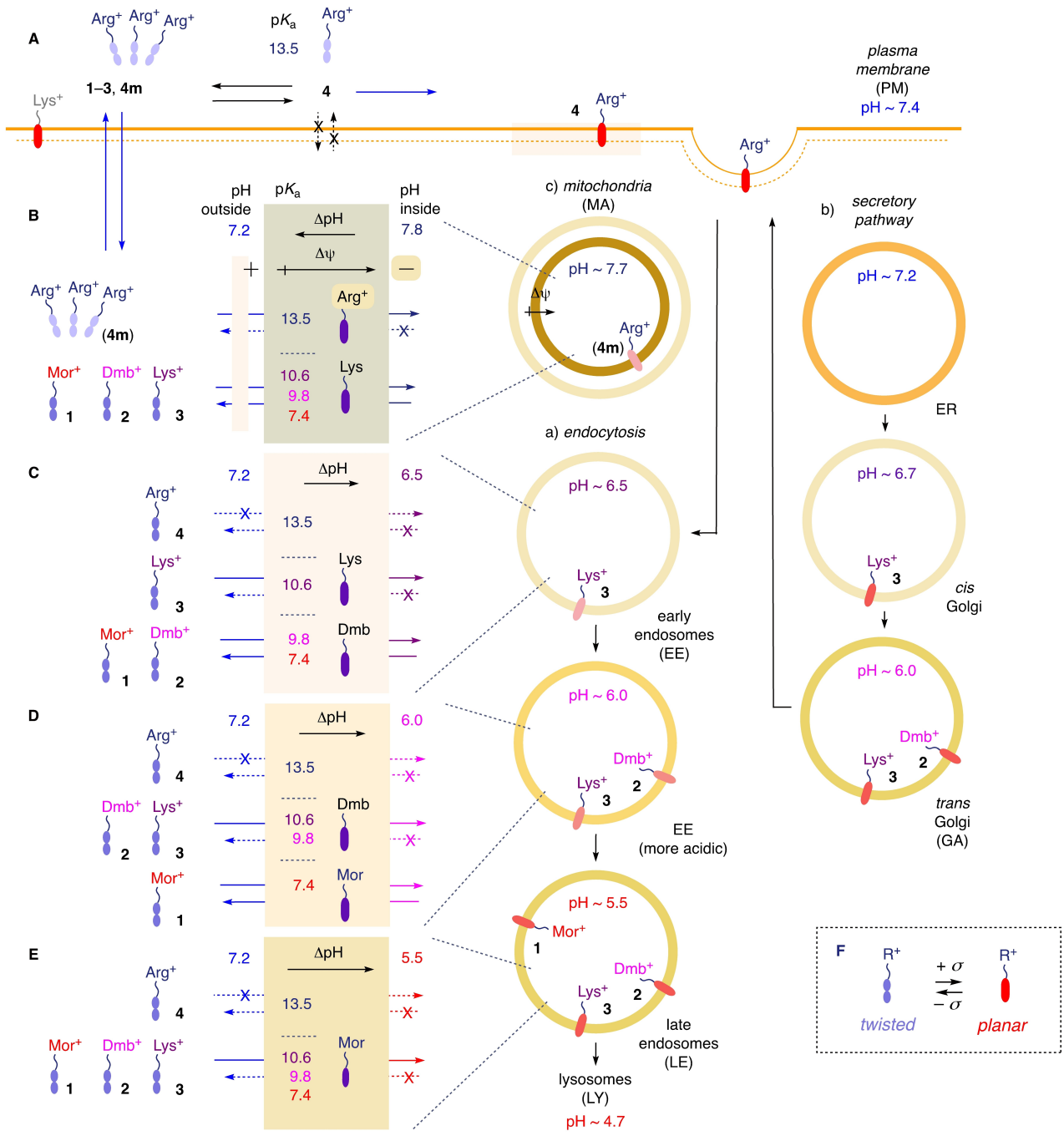

Figure 5. Tracking rules for cellular compartments according to the dynamic acidity of probes **1**–**4**, covering a) endocytosis, b) secretory pathway, and c) mitochondria. (A) Sufficiently acidic cationic probes (**1**-**3**) cross the plasma membrane by transient deprotonation; less acidic probes either label the PM (**4**) or cross it as CPP-like self-assembled micelles (**4 m**). (B) Probes with $pK_a \sim 13.5$ that cross the PM accumulate in mitochondria (**4 m**). (C) Due to unidirectional penetration across minimalist pH gradients, probes with $pK_a \sim 10.6$ completely label early endosomes, together with GA, LE and LY (**3**). (D) Probes with $pK_a \sim 9.8$ label early endosomes incompletely, together with mostly LE and LY. (E) Probes with $pK_a \sim 7.4$ label only LE and LY but neither early endosomes nor Golgi apparatus. (F) In their target membranes, flipper probes report order and tension (σ) by red shift and lifetime increase upon physical compression in the ground state (Figure 4).

Results and Discussion

Synthesis and characterization

The synthesis of flippers **1**, **2** and **5** has been reported.[81] Flippers **3** and **4** were prepared analogously by CuAAC (copper-catalyzed azide-alkyne cycloaddition) of alkyne flipper **6**, accessible in 14 steps from tetrabromothiophene **7**,[81] and the corresponding azides (Schemes 1, S1, S2). The synthesis of flipper **4** is shown as an example (Scheme 1). Aminohexylazide **9** was reacted with *S*-methylthiourea **10** to give protected guanidine azide **11**. After the removal of Boc groups, the

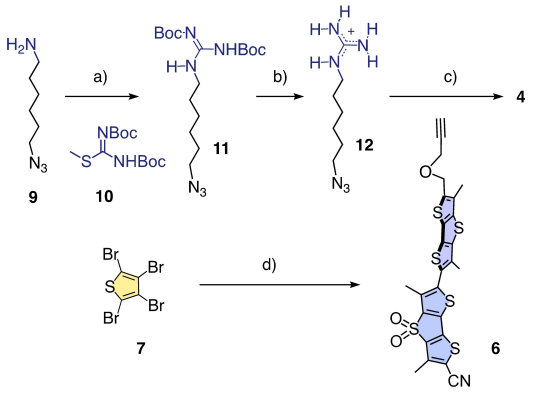

Scheme 1. Synthesis of Arg-Flipper **4**. a) Et_3N, CH_2Cl_2, 16 h, 73%. b) TFA, CH_2Cl_2, quant. c) $CuSO_4 5H_2O$, Na-ascorbate, TBTA, CH_2Cl_2, H_2O, MeOH, 1.5 h, 38%. d) 14 steps.[81]

obtained azide **12** underwent CuAAC with alkyne **6** to afford target molecule **4**.

Mor-Flippers

The morpholino (Mor) flipper **1** with $pK_a = 7.4$ has been reported to target lysosomes and late endosomes (Figure 5) with high selectivity and report on changes in membrane tension by changes in fluorescence lifetime.[58] Referred to here as Mor-Flipper **1** for consistency, it has been commercialized as Lyso-Flipper-TR® and has already been used to explore the mechanics of endocytosis.[81]

Dmb-Flippers

With $pK_a = 9.8$, the less acidic dimethoxybenzylamine (Dmb) flipper **2** has been shown to track also early endosomes besides late endosomes and lysosomes (Figure 5).[51] Changes in membrane tension in early endosomes were detectable by FLIM using masks made by co-localization with fluorescently labeled dextran (A647-Dextran) transiting through early endosomes.

Lys-Flippers

The headgroup of flipper probe **3** reproduces the side chain of lysine (Lys, Figure 4). The acidity of the primary alkyl ammonium cation is known to be at $pK_a = 10.6$.[82] This literature value was used in this study. The $pK_a = 10.6$ of Lys-Flipper **2** exceeds the $pK_a = 9.8$ of Dmb-Flipper **2** substantially. However, as outlined in the introduction, there is much support in the literature that the acidity of this ammonium cation should be sufficient to temporarily deprotonate at pH 7.2–7.4 to diffuse across the plasma membrane.[1–13] Indeed, many small molecule drugs are expected to reach their intracellular target by this mechanism.[6] The unidirectional penetration of early endosomes of Lys-Flipper **3** should thus be more efficient than with Dmb-Flipper **2** (Figure 5C, D), while the approaching edge of the dynamic range of acidity foretold a more complex behavior (Figure 5).

Intracellular tracking with Lys-Flipper **3** was explored by confocal laser scanning microscopy (CLSM) in HeLa Kyoto (HK) cells (Figure 6). CLSM images were characterized by bright puncta on an intense intracellular background (Figure 6A). The nature of the bright puncta was explored by co-localization with EGF labeled with Alexa-647 (Far-Red, FR). This probe binds to the EGF receptor (EGFR) and enters cells by endocytosis (Figure 5a), thus temporarily labeling early endosomes after 10 min (Figure 6B) and then moving on to label late endosomes one hour after addition.[51] Co-incubation of Lys-Flipper **3** with EGF-FR for 10 min showed excellent co-localization (Figures 6C, S2). In merged images with flipper emission colored in green (Figure 6A) and EGF-FR in red (Figure 6B, left), most of bright puncta turned yellow (Figure 6B, right). This qualitative impression was supported by automated high-content microscopy, which allows the quantitative analysis of many cells in a short time. The co-localization ratio was defined as the number of yellow (co-positive) puncta divided by the number of red (EGF-positive endosomes) puncta. The result confirmed that Lys-Flipper **3** labeled about 70% of all early endosomes, while the previous best Dmb-Flipper **2** labeled only about 45% (Figure 6C).[51] This result was in agreement with the expectation that the raised pK_a of Lys-Flipper **3** hinders the outward passage across the EE membrane to result in its retention despite the weak acidity of the EE interior (Figure 5C).

Compared to Dmb-Flipper **2** and particularly Mor-Flipper **1**,[51] Lys-Flipper **3** showed clearly more background fluorescence beyond the bright puncta of early endosomes, particularly near the nucleus (Figure 6A). According to the global tracking rules envisioned in this study, unidirectional penetration and thus retention in the Golgi apparatus (GA)

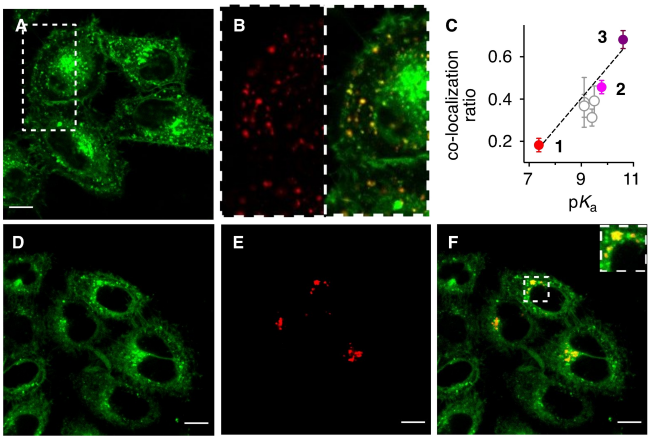

Figure 6. (A) CLSM images of HK cells labeled with Lys-Flipper **3** (green). (B) Zoomed area of (A) merged with EGF-FR after a 10 min pulse (right), with the EGF-FR channel for the zoomed area for comparison (red, left). (C) The ratio of EGF-FR labeled organelles (i.e., EE) co-localized with Lys-Flipper **3**, compared to Mor-Flipper **1**, Dmb-Flipper **2** and previously reported benzylamine flipper analogs with finetuned pK_a.[51] (D–F) CLSM images of HK cells expressing GFP-HaloTag on the membrane of Golgi apparatus (GTS-HaloTag-GFP, red, E) labeled with Lys-Flipper **3** (green, D) and merged (F). Scale bars = 10 μm.

could contribute to this additional fluorescence (Figure 5Cb) besides the obvious retention in late endosomes and lysosomes (Figure 5D,E). The luminal pH of the Golgi apparatus is similar to early endosomes and increases from pH 6.0 for *trans* GA to pH 6.7 for *cis* GA (Figure 5b).[59]

To explore this hypothesis, HK cells were transiently transfected to express GTS-HaloTag-meGFP in the Golgi apparatus.[83,84] After incubation of these cells with Lys-Flipper **3**, significant co-localization of the flipper (green, Figure 6D) and GFP emission (red, Figure 6E) was found (yellow, Figures 6F, S5). Most important was the absence of red areas in merged images, implying complete tracking of all GFP-labeled GA by Lys-Flipper **3** (Figure 6D). In reverse, GA labeling with GTS-HaloTag-meGFP was clearly incomplete, best visible with entire cells without GFP (Figure 6D vs 6E, missing red but not green). Incomplete GA labeling with GTS-HaloTag-meGFP was known to originate from incomplete transfection, with possible contributions also from specific localization of the expressed protein, GA fragmentation and other damage. The overall appearance of the Golgi apparatus in GTS-HaloTag-meGFP transfected HK cells was as observed previously.[84]

Besides dominant EE and GA tracking, Lys-Flipper **3** also labeled the plasma membrane weakly (Figure 6A, D). This minor retention in the plasma membrane decreased and disappeared within 30 minutes (Figure S12). Incubated at 4 °C, the disappearance of this partial plasma membrane (PM) labeling was slower (Figure S15). This minor temperature dependence did not imply that Lys-Flipper **3** enters cells and labels early endosomes through endocytosis. Temperature and time independent EE, GA, LE and LY labeling was clearly not consistent with the endocytic trafficking illustrated by EGF-FR (Figures 6B, right vs left side, S12). Several parameters were likely to contribute to the minor temperature dependence of the direct translocation across the plasma membrane by transient deprotonation of Lys-Flipper **3**, including the poor acidity of the linear alkyl ammonium cation, membrane reorganization, and so on.

To probe the generality of the proposed tracking rules, HeLa MZ and RPE1 cells were labeled with Lys-Flipper **3** together with Hoechst 33342 to stain the nucleus (Figure 7A, C). As in HK cells, bright puncta consistent with EE tracking were observed, together with background emission for the reasons described above. In the presence of bafilomycin A1, the puncta characteristic for EEs disappeared, and Lys-Flippers **3** distributed more randomly within the cells (Figure 7B, D). Bafilomycins are polyketide macrolactone natural products that target V-ATPase and thus inhibit acidification of lysosomes and endosomes.[85] Inhibition by bafilomycin A1 thus confirmed Lys-Flipper **3** of targeting early endosomes as expected from the proposed tracking rules, that is by unidirectional EE penetration along minimalist pH gradients.

The application of hyperosmotic stress to cells labeled with Lys-Flipper **3** shortened fluorescence lifetimes to the extent known for operational flipper probes, including Dmb-Flipper **2** (Figure 8A, B). Building on extensive precedence,[51,81] this observation implied that Lys-Flipper **3** is operational to image membrane tension in the tracked membranes (Figure 5F). FLIM images taken in planes outside the GA, LE and LY rich

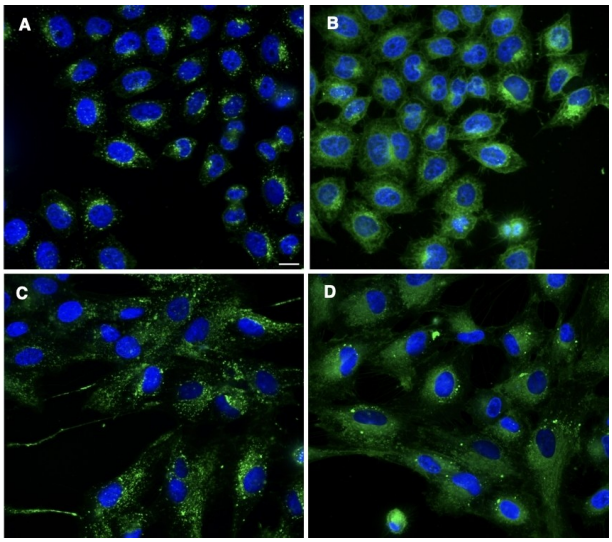

Figure 7. Spinning disk confocal microscopy images of HeLa MZ (A, B) and RPE1 cells (C, D) labeled with Lys-Flipper **3** (green) and Hoechst 33342 (blue) in the absence (A, C) and presence (B, D) of BafA1. Scale bars = 10 μm.

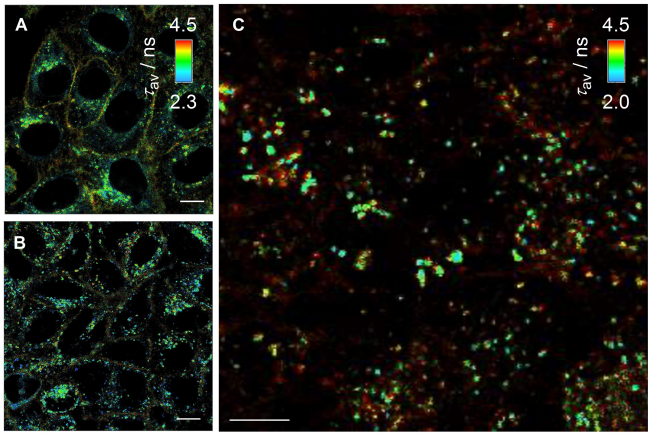

Figure 8. FLIM images of Lys-Flipper **3** (1.5 μM) under isotonic (A, τ_{av} = 3.53 ns; C) and hypertonic (B, τ_{av} = 3.38 ns) conditions, recorded at (A, B) and above (C) the nuclear plane. Scale bars = 10 μm.

perinuclear region allowed to focus lifetime recording on early endosomes (Figure 8C). Even more specific membrane tension imaging in early endosomes, if desired, is possible with masks, as illustrated previously for early endosomes with Dmb-Flipper **2** and masks generated from Alexa-647 Dextran.[51]

In summary, the rather complex staining pattern of Lys-Flipper **3** is in excellent agreement with its acidity at the edge of the dynamic range for membrane penetration in neutral water, that is, the universal tracking rules for unidirectional penetration elaborated in this study (Figure 5). Most importantly, Lys-Flipper **3** is found to track early endosomes much more efficiently (70%) than Dmb-Flipper **2** (45%) at preserved mechanosensitivity. This finding identifies Lys-Flipper **3** as an excellent probe to image the mechanics of early endocytosis, significantly superior to the previous best Dmb-Flipper **2**

(Figures 6C, 8C, 5C, B).[51,81] Additional GA labeling found for Lys-Flipper **3** is primarily of interest with regard to the completion and validation of tracking rules for unidirectional penetration (Figures 5, 6F). The importance of this approach for GA tracking for use in biology is questionable because the probes operate at the edge of the dynamic range of acidity, and more selective approaches to GA tracking operating with cysteine have been reported.[86–88] However, the possibility to track along the pH gradient of the Golgi apparatus with the pK_a gradient validated with **1**–**3** for endosomes could be worth further attention, depending on biological interest.[59] Weak plasma membrane labeling by Lys-Flipper **3**, finally, has no practical interest because plasma membrane staining is a solved problem.[81] However, weak plasma membrane labeling and its dependence on temperature and time are significant to outline tracking rules for unidirectional penetration comprehensively and are consistent with expectations in this context (Figure 5).

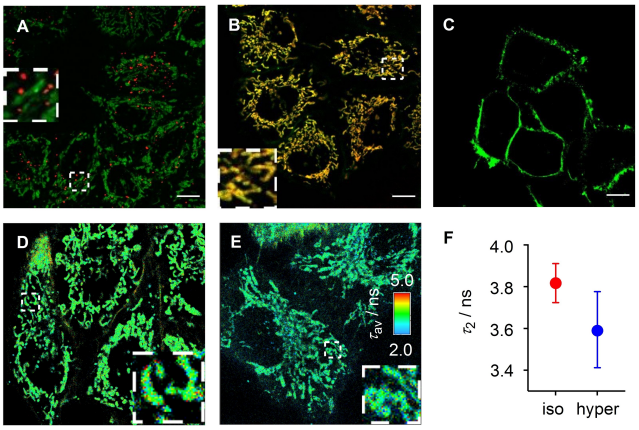

Figure 9. CLSM images of (A, B) HK cells labeled with Arg-Flipper **4** (1.5 μM, green) and merged with (A) EGF-FR (10 min after addition, red) or (B) MitoTracker Green™ (red), and (C) of HK cells 5 min after addition of Arg-Flipper **4** (0.5 μM). (D–F) FLIM images of Arg-Flipper **4** (1.5 μM) under isotonic (D, τ_{av} = 3.26 ns) and (E) hypertonic conditions (E, τ_{av} = 3.07 ns), with (F) lifetimes obtained. Scale bars = 10 μm.

Arg-Flippers

Flipper **4** contains a guanidinium cation, mimicking the side-chain of arginine (Arg, Figure 4). The acidity of this cation is expected to be at pK_a ~ 13.5.[25] However, as mentioned in the introduction, the determination of precise values is complicated by the coinciding deprotonation of water.[25] The literature value pK_a ~ 13.5 was used in this study.

Cellular imaging experiments with Arg-Flipper **4** were intriguing because probe localization changed dramatically depending on conditions that were difficult to control. This unusual behavior was in good agreement with expectations from the tracking rules for membrane penetration with cationic acids developed in this study (Figure 5).

Under certain conditions, including high concentrations (Figure S9), Arg-Flipper **4** readily crossed the plasma membrane and targeted inner organelles. Co-localization experiments with EGF-FR (red) were negative for EE tracking by Arg-Flipper **4** (green, Figures 9A, S4). In clear contrast, MitoTracker Green™ (red) showed an excellent co-localization ratio (Pearson Correlation Coefficient PCC = 0.9, Figure 9B). Upon depolarization of mitochondria using FCCP, Arg-Flipper **4** stopped tracking MC (Figure S8). Incubation at 4 °C, as well as a change of the pH of the medium during the incubation, did not change the localization of the probe but slightly increased the amount of probe retained in the plasma membrane (Figure S10, S17).

These results suggested that under the used conditions, Arg-Flipper **4** self-assembles into micelles **4m** that cross the plasma membrane by temperature-independent repulsion-driven ion pairing (Figure 5A), thus acting like non-covalent CPP mimics (Figure 2A). Concentration and condition dependent formation of small and usually non-fluorescent micelles by flipper amphiphiles in water is common and important for function since it minimizes background emission.[89] Arrived in the cytosol, Arg-Flipper micelles **4m** partially or fully disassemble due to dilution and unidirectionally penetrate mitochondria, driven by the FCCP-sensitive membrane potential. Images of mitochondria tracked with Arg-Flipper **4** were bright because the high pK_a ~ 13.5 prevented any possible temporary deprotonation even in the more basic interior of mitochondria (pH = 7.7, $\Delta pK_a \gg 3.5$; Figure 9). Mitochondria tracking and brightness with Arg-Flipper **4** were at least as good as with the quite extensively described and used Mito-Flipper-TR® **5**,[58,81] and responsiveness to changes in membrane tension in FLIM was intact (Figure 9D–F).

Variation of conditions, including lowering of the concentration, redirected Arg-Flipper **4** to the plasma membrane (Figure 9C). Slow internalization of the probe within around 30 minutes could be inhibited by lowering the temperature to 4 °C (Figures S13, S16). These results suggested that contrary to direct penetration of flipper micelles **4m**, monomeric flippers **4** that label the plasma membrane enter cells by endocytosis.

Interestingly, Arg-Flipper **4** could be observed to produce bright puncta in the plasma membrane, which then were ejected into the cells (Figure 10). These observations suggested that, reporting on membrane order and tension in FLIM images, Arg-Flipper **4** could be of interest to image mechanics of the initial steps of endocytosis. Arg-Flipper **4** co-localized partially with EGF-FR, especially in regions close to or still connected to the plasma membrane, indicating the Arg-Flipper **4** at least partially images endocytic vesicle formation (Figures 10A, C, E, S3).

Comparison of CLSM images for co-localization (Figure 10A, C, E) and FLIM images (Figure 10B, D, F) revealed that the bright puncta in the plasma membrane have a much shorter lifetime. Moreover, EGF-FR positive puncta had overall lower lifetime than EGF-FR negative puncta (e.g., Figure 10E; Ac, Cb vs 10F; Bc, Db). Although FRET between the flipper and EGF-FR could possibly account for such result, previous studies did not support this interpretation.[51] With short lifetimes reporting on low order and/or tension (Figure 5F), the short lifetime of EGF-FR negative puncta could thus reflect more lipid reorganization into disordered membrane domains,[90–93] while the even shorter

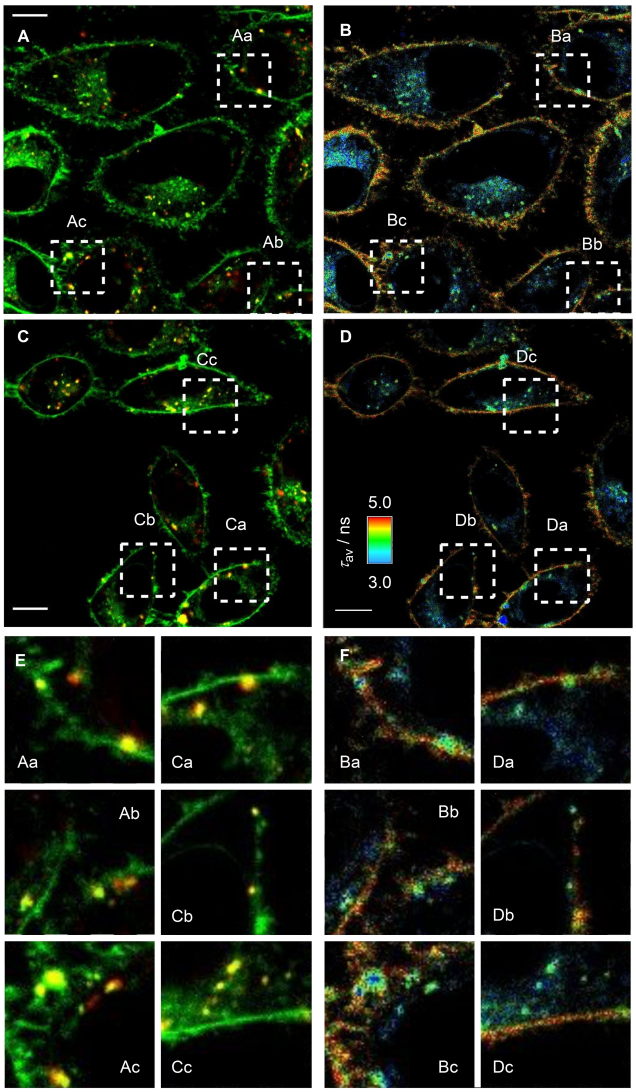

Figure 10. (A, C, E) CLSM images of HeLa Kyoto cells labeled with Arg-Flipper **4** (green) merged with EGF-FR (red) and (B, D, F) FLIM images of the flipper channel. Scale bars = 10 μm.

lifetime of EGF-FR positive puncta would then correctly report the low tension needed for the polymerization of membrane deforming machinery.[90–97] Consistent with this interpretation, puncta released from the membrane had overall lower lifetime than puncta at the plasma membrane (e.g., Figure 10E; Ca vs 10F; Da). These preliminary observations hint at the potential of Arg-Flipper **4** to image the mechanics of the first steps of endocytosis.

In summary, Arg-Flipper **4** labels either mitochondria or the plasma membrane and early events in endocytosis, depending on conditions during incubation. A shift toward plasma membrane labeling upon dilution supports that self-assembly into micelles accounts for mitochondria tracking and explains why switching selectivity is difficult to control. This complex behavior of Arg-Flipper **4** is in excellent agreement with the general tracking rules for unidirectional penetration of cationic acids elaborated in this study (Figure 5). With an acidity too weak to release protons in neutral water, monomeric flipper **4** cannot cross the plasma membrane by temporary neutralization and label the outer leaflet of the plasma membrane (Figure 5A). Micellar flippers **4m** cross the plasma membrane like CPPs by repulsion-driven ion pairing, unidirectionally penetrate mitochondria driven by the membrane potential and are well retained because they cannot deprotonate also in the more basic interior of mitochondria (Figure 5Bc). Mito-tracking by micellar **4m** is at least as selective and bright as with Mito-Flipper-TR® **5** and thus of interest in practice. Plasma membrane labeling is a solved problem. However, the unique partitioning of monomeric **4** into inward-detaching vesicles appears exceptionally promising to explore the mechanics of early stages in endocytosis.

Conclusion

Two complementary approaches exist for specific fluorescence labeling within cells. Cellular engineering with self-labeling proteins is attractive because it is universal and non-empirical.[98–101] Empirical tracking appeals because it is simple and user-friendly, small-molecule probes can just be added to cells without any engineering.[56–58,98–101] Because of their empirical nature, the molecular basis of tracking varies broadly. The unidirectional penetration of membranes along strong pH gradients and membrane potentials is known to account for the tracking of lysosomes and mitochondria, respectively.[51,81] These two trackers take advantage of extreme situations that are easy to control and understand. The chemical space between the two extremes is largely unexplored and centers around the question of the dynamic range of acidity. To map out this space, this study moves toward and beyond the edge of the dynamic range of acidity. The results are general tracking rules for fluorescent probes that operate by unidirectional penetration along pH gradients.

The obtained tracking rules are summarized in Figure 11. In brief, probe **1** with $pK_a \sim 7.4$ unidirectionally penetrates lysosomes and late endosomes (pH < 6.0) but not early endosomes (pH 6.0–6.5).[58] Probe **2** with $pK_a \sim 9.8$ labels also early endosomes, although only by 45%.[51] With $pK_a \sim 10.6$ in probe **3**, EE labeling increases to 70%, and also the Golgi apparatus is penetrated unidirectionally (pH 6.0–6.7). Probe **4** with $pK_a \sim 13.5$ fails to enter cells as monomers and thus labels the plasma membrane, particularly detaching vesicles entering endocytosis, but crosses the plasma membrane as CPP-like micelles **4m** and labels mitochondria attracted by the membrane potential. The observed good retention of probe **3** in early endosomes and the inability of the monomeric **4** to cross the plasma membrane are consistent with the dynamic range of acidity $\Delta pK_a = 3.5 \pm 0.3$ to penetrate membranes, deduced from the partial escape of **2** ($pK_a = 9.8$) from early endosomes (pH ~ 6.3). In the given context, this value can be considered as quite accurate because the pH within early endosomes ranges from ~6.0 to ~6.5. Flipper **2** thus should fail to enter early endosomes if the dynamic range would be $\Delta pK_a > 3.8$, while it should enter all early endosomes if $\Delta pK_a < 3.2$. However, it is understood that

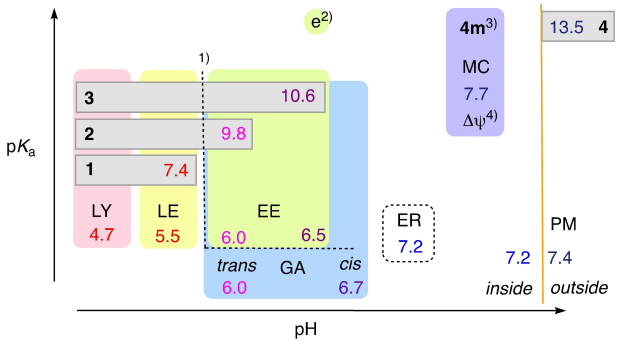

Figure 11. Tracking map for probes operating by unidirectional penetration, according to the pK_a of flippers **1**–**4** and their tracking of membranes with different internal pH. 1) Differentiation between EE and LE-LY-GA is possible by time-dependent co-localization with EGF-FR. 2) Vesicles detaching from PM detectable during slow endocytosis (e). 3) Probe **4** can cross PM and track mitochondria upon self-assembly into CPP-like micelles (**m**). 4) Unidirectional penetration controlled by potential, not pH gradient. LY = lysosomes, LE = late endosomes, EE = early endosomes, GA = Golgi apparatus, ER = endoplasmic reticulum, MC = mitochondria, PM = plasma membrane, compare Figure 5.

this quite precise dynamic range of acidity $\Delta pK_a = 3.5 \pm 0.3$ is limited to the present context. Structural variations of cations with constant pK_a = 9.8 will already change membrane penetration. Beyond penetrating membranes, acidified arginines with a pK_a ~8.0 have been mentioned in the introduction.[24] Similarly high $\Delta pK_a \sim 5.5$ has been observed for malonate esters by stabilization of their conjugate enolate bases with anion-π interactions.[102]

For practical use, access to EE tracking with 70% efficiency using pK_a ~10.6 in Lys-Flipper **3** is most interesting. Coinciding labeling of LE, LY and GA requires co-labeling analysis with EGF, which is, however, not further problematic.[51] Contrary to EE tracking through endocytosis of labeled ligands, EE tracking by unidirectional penetration is fast, independent of time and without probe immobilization on a receptor. Arg-Flipper **4** with pK_a ~13.5 shows promise in tracking mitochondria and particularly in imaging vesicle formation and detachment from the plasma membrane. Used together, Lys-Flipper **3** and Arg-Flipper **4** thus provide unique and promising tools to explore the mechanics of the early stages of endocytosis.

Contrary to this tracking of early endosomes with **3** and **4**, the tracking of plasma membrane and mitochondria are solved problems, and practical contributions from **4** are unlikely in this context. Established trackers also exist for the ER, which is not accessible with probes operating by unidirectional penetration.[56–58,99] The same presumably[86–88] also holds for GA tracking with **3**, although the possibility of variable *trans* selectivity from unidirectional penetration might be worth further attention (Figure 5b).[59] Independent of direct probe applications, the general objective of this study is of fundamental nature, that is, to contribute to a global understanding of probes that operate by unidirectional penetration. The results are expressed in general tracking rules for use in the community.

Experimental Section

Please see the Supporting Information.

The data that support the findings of this study are openly available: https://doi.org/10.5281/zenodo.6496765.

Acknowledgements

We thank D. Moreau and S. Vossio for help with high-content microscopy and analysis, M. Hensel (Osnabrück University) for providing materials, the NMR, the MS, the Bioimaging and ACCESS platforms for services, and the University of Geneva, the National Centre Chemical Biology (NCCR) Chemical Biology, the NCCR Molecular Systems Engineering and the Swiss NSF for financial support (Excellence Grant 200020 204175; 51NF40-185898; 51NF40-182895). Open access funding provided by Universite de Geneve.

Conflict of Interest

The authors declare no conflict of interest.

Keywords: cell-penetrating peptides · dynamic acidity · early endosomes · pH gradients · trackers · transmembrane translocation

[1] C. Tanford, J. G. Kirkwood, *J. Am. Chem. Soc.* **1957**, *79*, 5333–5339.
[2] D. Bashford, M. Karplus, *J. Phys. Chem.* **1991**, *95*, 9556–9561.
[3] M. L. Mugnai, D. Thirumalai, *J. Chem. Theory Comput.* **2021**, *17*, 1944–1954.
[4] L. Zanetti-Polzi, I. Daidone, A. Amadei, *J. Phys. Chem. B* **2020**, *124*, 4712–4722.
[5] P. A. Shore, B. B. Brodie, C. A. M. Hogben, *J. Pharmacol. Exp. Ther.* **1957**, *119*, 361–369.
[6] Z. Yue, C. Li, G. A. Voth, J. M. J. Swanson, *J. Am. Chem. Soc.* **2019**, *141*, 13421–13433.
[7] N. J. Gleason, V. V. Vostrikov, D. V. Greathouse, R. E. Koeppe, *Proc. Natl. Acad. Sci. USA* **2013**, *110*, 1692–1695.
[8] T. D. Machajewski, C.-H. Wong, *Angew. Chem. Int. Ed.* **2000**, *39*, 1352–1375; *Angew. Chem.* **2000**, *112*, 1406–1430.
[9] M. M. Müller, M. A. Windsor, W. C. Pomerantz, S. H. Gellman, D. Hilvert, *Angew. Chem. Int. Ed.* **2009**, *48*, 922–925; *Angew. Chem.* **2009**, *121*, 940–943.
[10] Z. C. Girvin, S. H. Gellman, *J. Am. Chem. Soc.* **2020**, *142*, 17211–17223.
[11] K. Johnsson, R. K. Allemann, H. Widmer, S. A. Benner, *Nature* **1993**, *365*, 530–532.
[12] B. Baumeister, A. Som, G. Das, N. Sakai, F. Vilbois, D. Gerard, S. P. Shahi, S. Matile, *Helv. Chim. Acta* **2002**, *85*, 2740–2753.
[13] D. P. Tieleman, J. Breed, H. J. C. Berendsen, M. S. P. Sansom, *Faraday Discuss.* **1999**, *111*, 209–223.
[14] R. Appel, S. Tacke, J. Klingauf, P. Besenius, *Org. Biomol. Chem.* **2015**, *13*, 1030–1039.
[15] N. M. Casellas, L. Albertazzi, S. Pujals, T. Torres, M. García-Iglesias, *Chem. Eur. J.* **2021**, *27*, 11056–11060.
[16] A. Méndez-Ardoy, J. R. Granja, J. Montenegro, *Nanoscale Horiz.* **2018**, *3*, 391–396.
[17] J. Cho, Y. Ishida, T. Aida, *Chem. Eur. J.* **2017**, *23*, 4818–4826.
[18] B. Dietrich, M. W. Hosseini, J. M. Lehn, R. B. Sessions, *J. Am. Chem. Soc.* **1981**, *103*, 1282–1283.
[19] T. M. Gloster, G. J. Davies, *Org. Biomol. Chem.* **2010**, *8*, 305–320.
[20] T. D. Heightman, A. T. Vasella, *Angew. Chem. Int. Ed.* **1999**, *38*, 750–770; *Angew. Chem.* **1999**, *111*, 794–815.

[21] V. L. Schramm, *ACS Chem. Biol.* **2013**, *8*, 71–81.
[22] K. U. Wendt, G. E. Schulz, E. J. Corey, D. R. Liu, *Angew. Chem. Int. Ed.* **2000**, *39*, 2812–2833; *Angew. Chem.* **2000**, *112*, 2930–2952.
[23] M. Watari, T. Ikuta, D. Yamada, W. Shihoya, K. Yoshida, S. P. Tsunoda, O. Nureki, H. Kandori, *J. Biol. Chem.* **2019**, *294*, 3432–3443.
[24] M. I. Niemeyer, F. D. González-Nilo, L. Zúñiga, W. González, L. P. Cid, F. V. Sepúlveda, *Proc. Natl. Acad. Sci. USA* **2007**, *104*, 666–671.
[25] C. A. Fitch, G. Platzer, M. Okon, B. Garcia-Moreno E, L. P. McIntosh, *Protein Sci.* **2015**, *24*, 752–761.
[26] N. Chuard, K. Fujisawa, P. Morelli, J. Saarbach, N. Winssinger, P. Metrangolo, G. Resnati, N. Sakai, S. Matile, *J. Am. Chem. Soc.* **2016**, *138*, 11264–11271.
[27] E. M. López-Vidal, C. K. Schissel, S. Mohapatra, K. Bellovoda, C.-L. Wu, J. A. Wood, A. B. Malmberg, A. Loas, R. Gómez-Bombarelli, B. L. Pentelute, *JACS Au.* **2021**, *1*, 2009–2020.
[28] S. J. Zamolo, T. Darbre, J.-L. Reymond, *Chem. Commun.* **2020**, *56*, 11981–11984.
[29] J. Rodríguez, J. Mosquera, J. R. Couceiro, J. R. Nitschke, M. E. Vázquez, J. L. Mascareñas, *J. Am. Chem. Soc.* **2017**, *139*, 55–58.
[30] Y.-C. Pan, A. Barba-Bon, H.-W. Tian, F. Ding, A. Hennig, W. M. Nau, D.-S. Guo, *Angew. Chem. Int. Ed.* **2021**, *60*, 1875–1882; *Angew. Chem.* **2021**, *133*, 1903–1910.
[31] A. Walrant, A. Bauzá, C. Girardet, I. D. Alves, S. Lecomte, F. Illien, S. Cardon, N. Chaianantakul, M. Pallerla, F. Burlina, A. Frontera, S. Sagan, *Biochim. Biophys. Acta* **2020**, *1862*, 183098.
[32] S. A. Bode, R. Wallbrecher, R. Brock, J. C. M. van Hest, D. W. P. M. Löwik, *Chem. Commun.* **2014**, *50*, 415–417.
[33] H. D. Herce, A. E. Garcia, M. C. Cardoso, *J. Am. Chem. Soc.* **2014**, *136*, 17459–17467.
[34] O. A. W. Haabeth, J. J. K. Lohmeyer, A. Sallets, T. R. Blake, I. Sagiv-Barfi, D. K. Czerwinski, B. McCarthy, A. E. Powell, P. A. Wender, R. M. Waymouth, R. Levy, *ACS Cent. Sci.* **2021**, *7*, 1191–1204.
[35] C. Douat, C. Aisenbrey, S. Antunes, M. Decossas, O. Lambert, B. Bechinger, A. Kichler, G. Guichard, *Angew. Chem. Int. Ed.* **2015**, *54*, 11133–11137; *Angew. Chem.* **2015**, *127*, 11285–11289.
[36] N. Laroui, M. Coste, D. Su, L. M. A. Ali, Y. Bessin, M. Barboiu, M. Gary-Bobo, N. Bettache, S. Ulrich, *Angew. Chem. Int. Ed.* **2021**, *60*, 5783–5787; *Angew. Chem.* **2021**, *133*, 5847–5851.
[37] T. Takeuchi, J. Montenegro, A. Hennig, S. Matile, *Chem. Sci.* **2011**, *2*, 303–307.
[38] T. Takeuchi, S. Matile, *J. Am. Chem. Soc.* **2009**, *131*, 18048–18049.
[39] J. Guo, T. Wan, B. Li, Q. Pan, H. Xin, Y. Qiu, Y. Ping, *ACS Cent. Sci.* **2021**, *7*, 990–1000.
[40] J.-P. Behr, *Acc. Chem. Res.* **2012**, *45*, 980–4.
[41] N. Pardi, M. J. Hogan, F. W. Porter, D. Weissman, *Nat. Rev. Drug Discovery* **2018**, *17*, 261–279.
[42] P. K. Hashim, K. Okuro, S. Sasaki, Y. Hoashi, T. Aida, *J. Am. Chem. Soc.* **2015**, *137*, 15608–15611.
[43] C. Gehin, J. Montenegro, E.-K. Bang, A. Cajaraville, S. Takayama, H. Hirose, S. Futaki, S. Matile, H. Riezman, *J. Am. Chem. Soc.* **2013**, *135*, 9295–9298.
[44] J. Zhou, L. Sun, L. Wang, Y. Liu, J. Li, J. Li, J. Li, H. Yang, *Angew. Chem. Int. Ed.* **2019**, *58*, 5236–5240; *Angew. Chem.* **2019**, *131*, 5290–5294.
[45] J. M. Priegue, D. N. Crisan, J. Martínez-Costas, J. R. Granja, F. Fernandez-Trillo, J. Montenegro, *Angew. Chem. Int. Ed.* **2016**, *55*, 7492–7495; *Angew. Chem.* **2016**, *128*, 7618–7621.
[46] A. Panahi, C. L. Brooks, *J. Phys. Chem. B* **2015**, *119*, 4601–4607.
[47] V. Gorteau, G. Bollot, J. Mareda, S. Matile, *Org. Biomol. Chem.* **2007**, *5*, 3000–3012.
[48] F. Kamp, J. A. Hamilton, *Proc. Natl. Acad. Sci. USA* **1992**, *89*, 11367–11370.
[49] E. N. W. Howe, P. A. Gale, *J. Am. Chem. Soc.* **2019**, *141*, 10654–10660.
[50] C. L. Andrew, A. R. Klemm, J. B. Lloyd, *Biochim. Biophys. Acta* **1997**, *1330*, 71–82.
[51] F. Piazzolla, V. Mercier, L. Assies, N. Sakai, A. Roux, S. Matile, *Angew. Chem. Int. Ed.* **2021**, *60*, 12258–12263; *Angew. Chem.* **2021**, *133*, 12366–12371.
[52] M. Li, H. Ge, V. Mirabello, R. L. Arrowsmith, G. Kociok-Köhn, S. W. Botchway, W. Zhu, S. I. Pascu, T. D. James, *Chem. Commun.* **2017**, *53*, 11161–11164.
[53] F. Miao, S. Uchinomiya, Y. Ni, Y.-T. Chang, J. Wu, *ChemPlusChem* **2016**, *81*, 1209–1215.
[54] K. Zhou, Y. Wang, X. Huang, K. Luby-Phelps, B. D. Sumer, J. Gao, *Angew. Chem. Int. Ed.* **2011**, *50*, 6109–6114; *Angew. Chem.* **2011**, *123*, 6233–6238.
[55] A. Wallabregue, D. Moreau, P. Sherin, P. Moneva Lorente, Z. Jarolímová, E. Bakker, E. Vauthey, J. Gruenberg, J. Lacour, *J. Am. Chem. Soc.* **2016**, *138*, 1752–1755.
[56] N. Wagner, M. Stephan, D. Höglinger, A. Nadler, *Angew. Chem. Int. Ed.* **2018**, *57*, 13339–13343; *Angew. Chem.* **2018**, *130*, 13523–13527.
[57] D. I. Danylchuk, P.-H. Jouard, A. S. Klymchenko, *J. Am. Chem. Soc.* **2021**, *143*, 912–924.
[58] A. Goujon, A. Colom, K. Straková, V. Mercier, D. Mahecic, S. Manley, N. Sakai, A. Roux, S. Matile, *J. Am. Chem. Soc.* **2019**, *141*, 3380–3384.
[59] P. Paroutis, N. Touret, S. Grinstein, *Physiology* **2004**, *19*, 207–215.
[60] T. Myochin, K. Kiyose, K. Hanaoka, H. Kojima, T. Terai, T. Nagano, *J. Am. Chem. Soc.* **2011**, *133*, 3401–3409.
[61] S. Takahashi, Y. Kagami, K. Hanaoka, T. Terai, T. Komatsu, T. Ueno, M. Uchiyama, I. Koyama-Honda, N. Mizushima, T. Taguchi, H. Arai, T. Nagano, Y. Urano, *J. Am. Chem. Soc.* **2018**, *140*, 5925–5933.
[62] Y. Wang, C. Wang, Y. Li, G. Huang, T. Zhao, X. Ma, Z. Wang, B. D. Sumer, M. A. White, J. Gao, *Adv. Mater.* **2017**, *29*, 1603794.
[63] K. Zhou, H. Liu, S. Zhang, X. Huang, Y. Wang, G. Huang, B. D. Sumer, J. Gao, *J. Am. Chem. Soc.* **2012**, *134*, 7803–7811.
[64] N. Narayanaswamy, K. Chakraborty, A. Saminathan, E. Zeichner, K. Leung, J. Devany, Y. Krishnan, *Nat. Methods* **2019**, *16*, 95–102.
[65] K. Leung, K. Chakraborty, A. Saminathan, Y. Krishnan, *Nat. Nanotechnol.* **2019**, *14*, 176–183.
[66] H. J. Kim, C. H. Heo, H. M. Kim, *J. Am. Chem. Soc.* **2013**, *135*, 17969–17977.
[67] A. Méndez-Ardoy, J. J. Reina, J. Montenegro, *Chem. Eur. J.* **2020**, *26*, 7516–7536.
[68] D. Asanuma, Y. Takaoka, S. Namiki, K. Takikawa, M. Kamiya, T. Nagano, Y. Urano, K. Hirose, *Angew. Chem. Int. Ed.* **2014**, *53*, 6085–6089; *Angew. Chem.* **2014**, *126*, 6199–6203.
[69] M. Tian, C. Liu, B. Dong, Y. Zuo, W. Lin, *Chem. Commun.* **2019**, *55*, 10440–10443.
[70] C. Benitez-Martin, J. A. Guadix, J. R. Pearson, F. Najera, J. M. Perez-Pomares, E. Perez-Inestrosa, *ACS Sens.* **2020**, *5*, 1068–1074.
[71] X. Liu, Y. Su, H. Tian, L. Yang, H. Zhang, X. Song, J. W. Foley, *Anal. Chem.* **2017**, *89*, 7038–7045.
[72] A. Jiménez-Sánchez, E. K. Lei, S. O. Kelley, *Angew. Chem. Int. Ed.* **2018**, *57*, 8891–8895; *Angew. Chem.* **2018**, *130*, 9029–9033.
[73] D. Pendin, R. Norante, A. De Nadai, G. Gherardi, N. Vajente, E. Basso, N. Kaludercic, C. Mammucari, C. Paradisi, T. Pozzan, A. Mattarei, *Angew. Chem. Int. Ed.* **2019**, *58*, 9917–9922; *Angew. Chem.* **2019**, *131*, 10022–10027.
[74] L. Yu, J. F. Zhang, M. Li, D. Jiang, Y. Zhou, P. Verwilst, J. S. Kim, *Chem. Commun.* **2020**, *56*, 6684–6687.
[75] C. Wang, M. Taki, Y. Sato, Y. Tamura, H. Yaginuma, Y. Okada, S. Yamaguchi, *Proc. Natl. Acad. Sci. USA* **2019**, *116*, 15817–15822.
[76] J. Santo-Domingo, N. Demaurex, *J. Gen. Physiol.* **2012**, *139*, 415–423.
[77] B. Baumeister, S. Matile, *Chem. Eur. J.* **2000**, *6*, 1739–1749.
[78] A. Fin, A. Vargas Jentzsch, N. Sakai, S. Matile, *Angew. Chem. Int. Ed.* **2012**, *51*, 12736–12739; *Angew. Chem.* **2012**, *124*, 12908–12911.
[79] J. García-Calvo, J. López-Andarias, N. Sakai, S. Matile, *Helv. Chim. Acta* **2022**, *105*, e202100238.
[80] J. García-Calvo, J. López-Andarias, J. Meillard, V. Mercier, C. Roffay, A. Roux, A. Fürstenberg, N. Sakai, S. Matile, *Chem. Sci.* **2022**, *13*, 2086–2093.
[81] L. Assies, J. García-Calvo, F. Piazzolla, S. Sanchez, T. Kato, L. Reymond, A. Goujon, A. Colom, J. López-Andarias, K. Straková, D. Mahecic, V. Mercier, M. Riggi, N. Jiménez-Rojo, C. Roffay, G. Licari, M. Tsemperouli, F. Neuhaus, A. Fürstenberg, E. Vauthey, S. Hoogendoorn, M. Gonzalez-Gaitan, A. Zumbuehl, K. Sugihara, J. Gruenberg, H. Riezman, R. Loewith, S. Manley, A. Roux, N. Winssinger, N. Sakai, S. Pitsch, S. Matile, *Chimia* **2021**, *75*, 1004–1011.
[82] H. K. Hall, *J. Am. Chem. Soc.* **1957**, *79*, 5441–5444.
[83] V. Liss, B. Barlag, M. Nietschke, M. Hensel, *Sci. Rep.* **2015**, *5*, 17740.
[84] K. Straková, J. López-Andarias, N. Jiménez-Rojo, J. E. Chambers, S. J. Marciniak, H. Riezman, N. Sakai, S. Matile, *ACS Cent. Sci.* **2020**, *6*, 1376–1385.
[85] F. Marceau, C. Roy, J. Bouthillier, *Methods Enzymol.* **2014**, *534*, 119–131.
[86] S. Sawada, A. Nakamura, T. Yoshii, K. Kuwata, F. Nakatsu, S. Tsukiji, *Chem. Commun.* **2020**, *56*, 15422–15425.
[87] W. Zhang, J. Zhang, P. Li, J. Liu, D. Su, B. Tang, *Chem. Sci.* **2019**, *10*, 879–883.
[88] R. S. Li, P. F. Gao, H. Z. Zhang, L. L. Zheng, C. M. Li, J. Wang, Y. F. Li, F. Liu, N. Li, C. Z. Huang, *Chem. Sci.* **2017**, *8*, 6829–6835.

[89] M. Macchione, N. Chuard, N. Sakai, S. Matile, *ChemPlusChem* **2017**, *82*, 1062–1066.
[90] M. Kaksonen, A. Roux, *Nat. Rev. Mol. Cell Biol.* **2018**, *19*, 313–326.
[91] G. M. I. Redpath, V. M. Betzler, P. Rossatti, J. Rossy, *Front. Cell Dev. Biol.* **2020**, *8*.
[92] L. Pelkmans, *Biochim. Biophys. Acta* **2005**, *1746*, 295–304.
[93] L. Johannes, S. Mayor, *Cell* **2010**, *142*, 507–510.
[94] M. Saleem, S. Morlot, A. Hohendahl, J. Manzi, M. Lenz, A. Roux, *Nat. Commun.* **2015**, *6*, 6249.
[95] U. Djakbarova, Y. Madraki, E. T. Chan, C. Kural, *Biol. Cell* **2021**, *113*, 344–373.
[96] M. Riggi, C. Bourgoint, M. Macchione, S. Matile, R. Loewith, A. Roux, *J. Cell Biol.* **2019**, *218*, 2265–2276.
[97] D. Lachowski, C. Matellan, S. Gopal, E. Cortes, B. K. Robinson, A. Saiani, A. F. Miller, M. M. Stevens, A. E. del Río Hernández, *ACS Nano* **2022**, *16*, 4322–4337.
[98] J. Liu, Z. Cui, *Bioconjugate Chem.* **2020**, *31*, 1587–1595.
[99] J. López-Andarias, K. Eblighatian, Q. T. L. Pasquer, L. Assies, N. Sakai, S. Hoogendoorn, S. Matile, *Angew. Chem. Int. Ed.* **2022**, *61*, e202113163; *Angew. Chem.* **2022**, *134*, e202113163.
[100] P. Gao, W. Pan, N. Li, B. Tang, *Chem. Sci.* **2019**, *10*, 6035–6071.
[101] N. Trinh, K. A. Jolliffe, E. J. New, *Angew. Chem. Int. Ed.* **2020**, *59*, 20290–20301; *Angew. Chem.* **2020**, *132*, 20466–20479.
[102] F. N. Miros, Y. Zhao, G. Sargsyan, M. Pupier, C. Besnard, C. Beuchat, J. Mareda, N. Sakai, S. Matile, *Chem. Eur. J.* **2016**, *22*, 2648–2657.

Manuscript received: April 4, 2022
Revised manuscript received: May 9, 2022
Accepted manuscript online: May 10, 2022
Version of record online: May 24, 2022